INTERNATIONAL JOURNAL OF APPLIED SCIENCE ENGINEERING AND MANAGEMENT

IJASEM

www.ijasem.org

Tribology in Industry Mechanical and Tribological Properties Evolution of [Si3N4/Al2O3]n Multilayer Coatings

A SANTOSH[1,2,3,4], Dr V VENUGOPAL[1,2,3,4], K KRISHNAVENI[1,2,3,4], RAHUL PATIL[1,2,3,4]

ABSTACT

With their fascinating features, multilayer coatings [Si3N4/Al2O3]n have attracted much attention in the food and pharmaceutical sectors. They might be used in a variety of operations. Unfortunately, there are no robust tribological investigations on this multilayer system based on [Si3N4/Al2O3]n that might emphatically represent its unique tribological properties. In order to better understand how the mechanical and tribological characteristics of [Si3N4/Al2O3]n coatings change with increasing bilayer numbers, this work focused on the tribological properties in both a dry and lubricated environment for n=1, 10, 30, and 70. A reduction of 33 percent in friction coefficient and a rise of 8.8% in lubrication efficiency were found when the number of bilayers was raised from 1 to 70, while the hardness and elastic modulus rose by 29 and 6.3%, respectively. This research found that the coating [Si3N4/Al2O3]70 has perfect qualities that make it a good option for use as a protective coating for food and pharmaceutical processing equipment.

INTRODUCTION

High-performance materials are needed to keep up with the ever-growing demand for industrial goods throughout the world, as well as to keep up with industry competition [1–2]. As a result, tribologically compatible coatings with high wear resistance and low friction are needed, as are components and tools coated with single layers or multilayers of coatings that can endure harsh conditions and give extended service lives [3-10]. In the literature, many single layer coating materials with the purpose of increasing mechanical properties have been reported, such as Si3N4, which has been used in various metalworking applications due to its high resistance, low thermal conductivity, and inter chemical behaviour in aggressive environments [11, 12]. Al2O3 has also been described as a single layer coating material with high hardness, good chemical stability, and refractory properties. Al2O3 Surfaces subjected to frictional wear and erosion by solid particles, as well as surfaces subjected to high temperatures, are good candidates for this material [13]. Multilayer systems, such as [TiN/ZrN], [TiAlN/TiN], and many more, have been demonstrated to be superior than typical single layer systems, bringing together the best properties of several layers, such as [TiN/TiAlN]. Multilayer structures with symmetry breaches between the layers increase the mechanical and tribological properties of materials by decreasing fracture propagation. Due to its outstanding mechanical, morphological, and tribological qualities, [Si3N4/Al2O3]n has attracted considerable attention as a prospective coating for processing equipment and cutting tools in several sectors.

Professor[1,2,3,4], Assistant professor[1,2,3,4],
Department of Mechanical Engineering,
Pallavi Engineering College,
Kuntloor(V),Hayathnagar(M),Hyderabad,R.R.Dist.-501505
amgothsanthosh001@gmail.com, rahulpatiljkd@gmail.com

However, there are no comprehensive tribological experiments on this multilayer system to illustrate its potential and unique properties when in interaction with other materials. Similar to this, there is little record of tribological tests conducted in a variety of situations, such as lubricated or high-temperature settings Therefore, the goal of this study was to investigate the mechanical characteristics of [Si3N4/Al2O3]n multilayer coatings as a function of the bilayer number n=1, 10, 30, and 70, as well as the tribological properties in a dry and lubricated environment. As a consequence, the multilayer coating was shown to be a viable material for use in the food and pharmaceutical sectors on a scientific foundation.

EXPERIMENTAL SECTION

Materials The AISI 316 steel substrates were obtained in cylindrical form with a diameter of ½ inch and a thickness of 5 mm. These substrates were then prepared superficially with sandpaper (SiC) in the order 80, 100, 240, 320, 400, 600, 800, 1000 and 1200 μm. After processing, they were polished in a metallographic polisher using an alumina water-solution of 1 and 0.3 μm. Finally, an alcohol ultrasound cleaning was carried out utilising a "Rio Grande UD50SH-2L" equipment for 10 minutes to eliminate residues on their surface. Monocrystalline silicons with an orientation (100) were also employed as substrates. The cathodes utilised were (Si-N) and (Al-O) both cathodes with a purity of 99.9 percent purchased from the business "PLASMATERIALS". Argon and Nitrogen were employed as precursor gases, each with a purity of 99.9 percent .

Coating Deposition

All coatings were deposited on silicon (100) and AISI 316 steel substrates by employing a multitarget magnetron reactive sputtering system, with an r.f. source (13.56 MHz) and two targets, Si-N and Al-O with 10 cm of diameter. The deposition parameters employed were a sputtering system with one target of Si-N and one of Al-O facing each other, the power applied to the Si-N target was 500W and 400W for the Al-O target; substrate– target distance was 7 cm and substrate temperature 300 ℃. The substrate was under circular rotation at 60 RPM to assist the production of the stoichiometric binary coating. The

substrates utilised offered a disk-type shape with 2 cm in diameter. The sputtering gas was a combination of Ar (50 sccm) and N2 (16 sccm) with a total operating pressure of 6×10−3 mbar. An unbalanced r.f. bias voltage was supplied, creating a negative signal set at −20 V. Moreover, the magnetron sputtering system contains a substrate positioning system in respect to the target spot and with an opening and shutting system that regulates the shutters functioning. This parameter permitted the altering of the bilayer number (n) ranging from 1, 10, 30, and 70; Therefore, it was feasible to modify the bilayer period (Λ) for all the coatings owing to the growth of the bilayer number while keeping a constant total coating thickness (2 μm)

Coating characterization technique

In a step type setup, the coatings were coated on half of the silicon substrate's (100) surface and measured using a KLA Tencor D-120 Profilometer. For each coating, 4 scans were done, with each step being 5 mm long. PANalytical X'Pert PRO diffractometer with Cu K radiation (1.5406) at Bragg–Brentano configuration (/2) at high-angle, three samples were used for each coating. XRD was performed using three samples for each coating. Each coating was investigated using a JSM 6490LV scanning electron microscope, which measured the bilayer periods of the multilayers. Multiple X-ray photoelectron spectroscopy (XPS) studies were performed on the n-layer [Si3N4/Al2O3]. Single layers of Si3N4 and Al2O3 were analysed using an ESCAPHI 5500 monochromatic Al K radiation with a passing energy of 0.01 eV to evaluate the chemical composition and the bonding of silicon and oxygen atoms. Three samples for each coating were utilised to produce a satisfactory result. Asylum Research MFP-3D® atomic force microscope (AFM) and a Scanning Probe Image Processor (SPIP) were used to measure the roughness and grain size of all coatings. We utilised three samples of each coating with an evaluated surface area of 5.0 m x m and this software was used to analyse and show the results. It is now the de facto standard for image processing in nanoscales because of its widespread usage. A diamond Berkovich tip and a Ubi1-Hysitron device were used to conduct nanoindentation mechanical studies at various stresses. For each coating, 3 samples were utilised in which their respective indentation matrices were produced, as shown in the

figure 9. These findings were analysed using the Oliver and Pharr technique [21], and for each coating, 3 samples were employed. Using a Microtest MT 4001-98 tribometer with a 6 mm diameter 100Cr6 steel pin as the sliding pattern, the applied load was 5 N in a total travel distance of 300 m, with an angular speed of 160 rpm for the [Si3N4/Al2O3]n multilayer systems. As part of a study on friction coefficients, pin-on-disk techniques were used in lubricated and non-lubricated environments to measure the sliding distances and bilayer numbers. Tests were carried out using hardened 100Cr6 steel balls in order to imitate an industrial process where the surface of a multilayer and the surface of hardened steel come into contact, as is the case in tribology. There is an FMO 85-AW (lubricant) from LUBRIPLATE that is suitable for lubrication of machinery and equipment that may come into contact with food, drink goods, or pharmaceuticals during manufacturing operations. Each coating was tested in a lubricated and a non-lubricated environment to provide valid statistical findings. In accordance with ASTM G171-03 [23], a Scratch Test Microtest MTR was utilised to conduct the scratch test. A sliding distance of 6 mm, a load of 0–90 N, and a feed rate of 1.97 mm/min were used in the test to provide a trustworthy result. A KLA Tencor D-120 profilometer was used to produce photographs of friction wear for all of the coatings, which had a 2 m thickness. A ZYGO New View 200 optical interferometer was also utilised to examine the wear track of each sample used in the tribological testing.

RESULTS AND DISCUSSION

Structural analysis (DRX)

Depending on the number of bilayers, the diffraction patterns for [Si3N4/Al2O3]n multilayers may be shown in Figure 1a. All coatings had a hexagonal crystal structure with the spatial group p63/m, as shown by the intensities of preferred orientations (101), (201), (209), (2013), (410) and (317) for 2 = 33.36°, 40.77 °, 54.54 °, 64 °, 66 °, and 76 ° respectively. There are indexing files (JCPDC) corresponding to these diffraction patterns at the International Center for Diffraction Data (00-009-0259) and (00-002-0921). (ICDD). A increased number of crystallites aligned in the preferred orientation, notably in the (101) and (209) planes, may have contributed to this increase of intensity. Figure 1b depicts a close-up of Si3N4 in the (101)

plane (higher intensity) and the location where the structure would be stress-free (dotted line). Peaks in the stress-free position (dotted line) may be noticed as the number of bilayers grows, showing the deposition process's relaxation of the tensile tensions. Close-up of the (209) plane corresponding to Al2O3 and the stress-free posture is shown in the figure 1c (dotted line). A movement to the right indicates an increase in compressive stress in the structure as the number of bilayers rises. As seen in figure 10, the mechanical characteristics will rise as a result of these stresses.

(a)

(b)

(b)

(c)
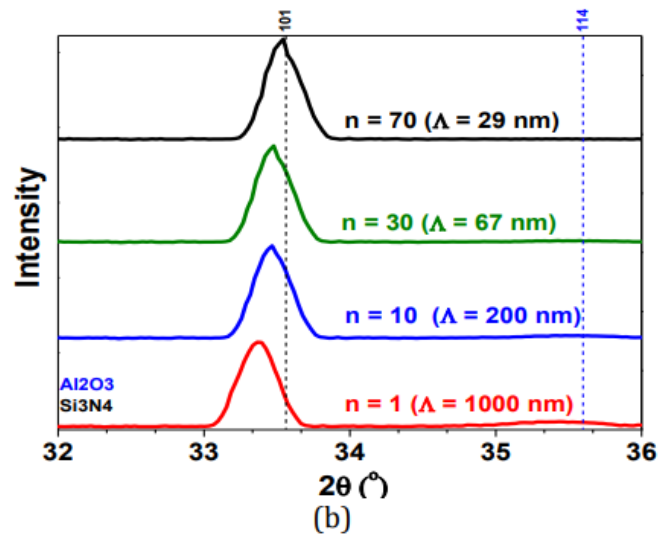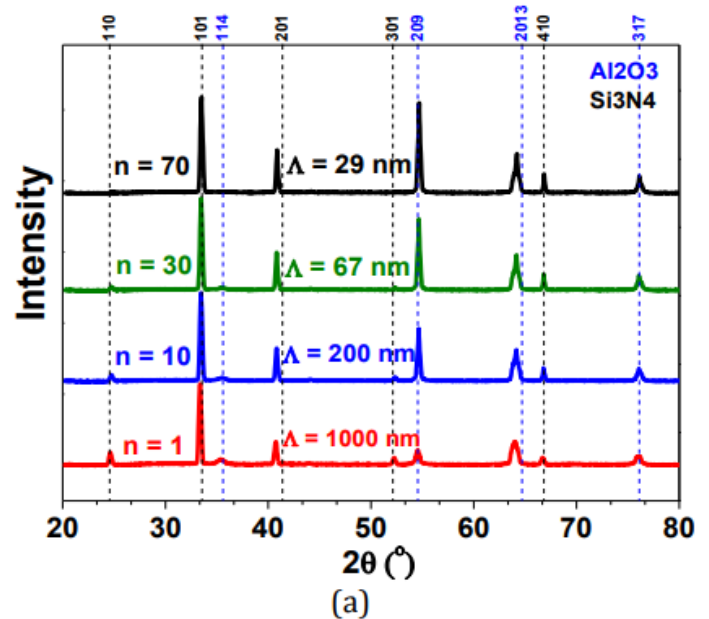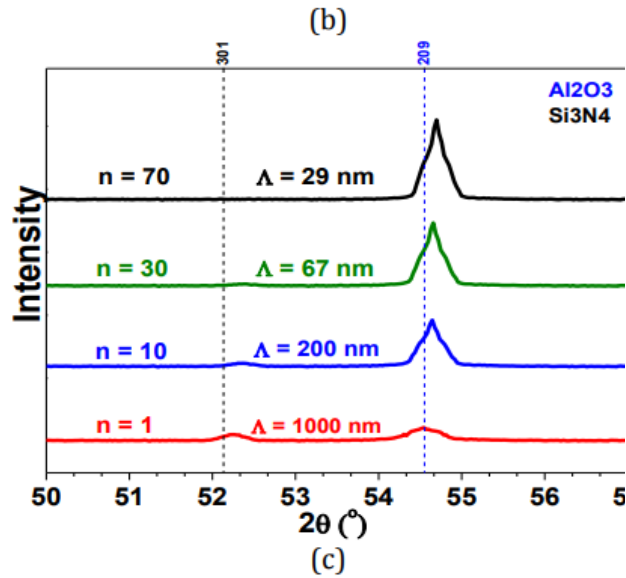
Diffraction patterns for [Si3N4/Al2O3]n multilayers: (a) the number of bilayers, (b) the preferred orientation (101) and (c) the diffraction pattern as a function of bilayer number (209)

X-ray Photoelectron Spectroscopy

In addition to Si(2p) and N(1s), but also O(1s), which may have been caused by sample contamination, is seen in the XPS spectra of the Si3N4 coating.. It is now easier to determine how much Si-N is in each layer, as well as which bonding configurations are most likely. In addition, the Si–N coatings' chemical composition and bonding characteristics are revealed in the core electronic spectra. The concentrations of Si and N elements in the Si-N layer may be determined by integrating the N(1s) and Si(2p) spectra adjusted for relevant sensitivity variables. Using the corresponding integral of the deconvoluted peaks, equation (1) may be utilised to determine the bond content [24, 25].

$$C_i = \sum(A_i/S_i)/\sum(A_j/S_{ij})$$

S is the sensitivity factor, A is the sum of the deconvoluted peaks, and C is the atomic content of the sample. The denominator is the total of all kinds of bonds decomposed from the whole peak of the sample's Si(2p) and N(1s) spectra, whereas the numerator is the sum of the integral of a single type of bond. The atomic concentrations of Si43 and N57 were found in the Si-N material. The O content was less than 2% in all of the Si-N films analysed.
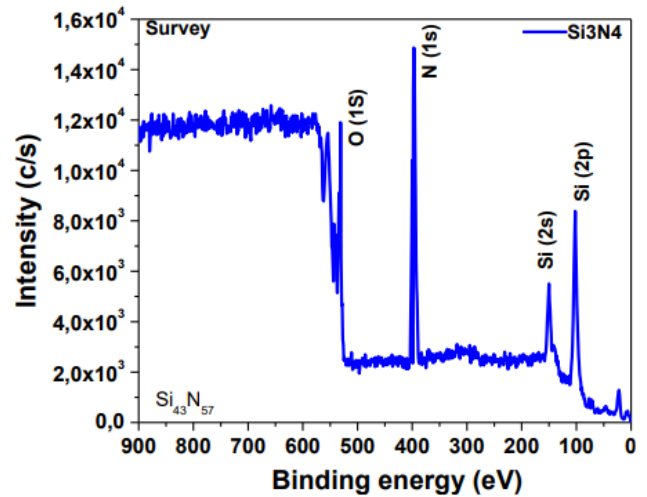

Analysis of a Si–N coating on a Si substrate with an R.f. negative bias voltage of around 20 V was performed using the scanning electron microscope (SEM). Figures 3a and 3b show high-resolution spectra for N(1s) and Si(2p), respectively, that have been modified using Gaussian functions to examine the surface stoichiometry in detail. The N-O bond was found to be situated at 400.6 eV in the high-resolution spectra of N(1s) [4, 5]. For example, 396.6 eV corresponds to the N-Si bond, whereas 394.4 eV may be assigned to the multiple chemical states of N owing to its diverse bond arrangements with adjacent atoms[6]. There were two peaks in the high-resolution spectra for Si(2p) that corresponded to the Si-O bond, which is in accord with another author [7, 8].
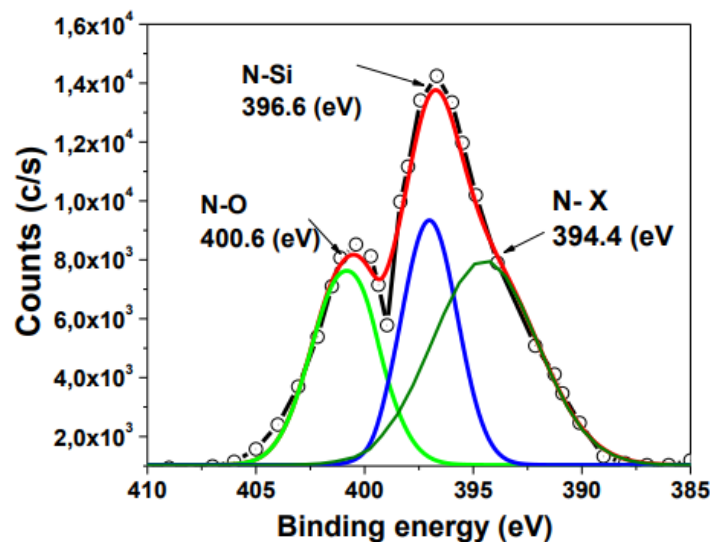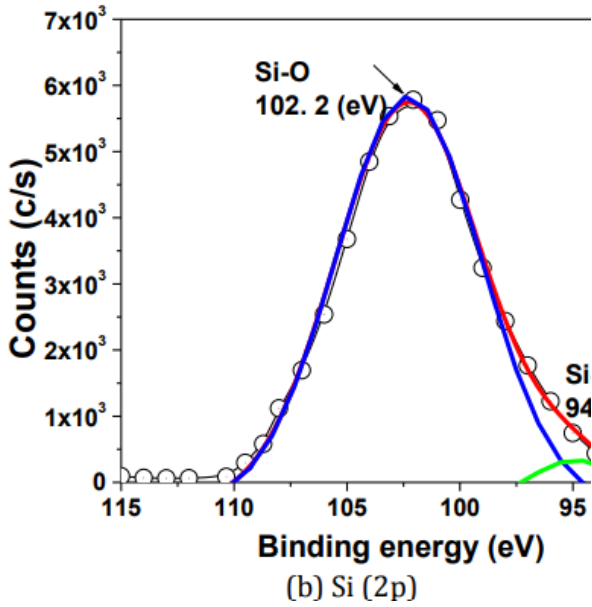
(b) Si (2p)

(a) N(1s) and (b) Si(2p) spectra from the coating of Si–N. According to the XPS literature about Al-O materials [13, 26], when the peaks are fitted from experimental results, it is necessary to first adjust the O energy band because it is the element that provides greater reliability for the XPS, then, take that first adjustment as base and, the other peaks related to the remaining elements are adjusted. Insulating materials (coatings) of this sort are essential because of their ability to resist charging and changes in the Fermi energy, hence eliminating the aforementioned uncertainties. Al(1s) and O(1s) are discovered in the XPS spectrum of the Al-O coating, as shown in Fig. 4. Al-O material yielded atomic concentrations of Al39 and O61.
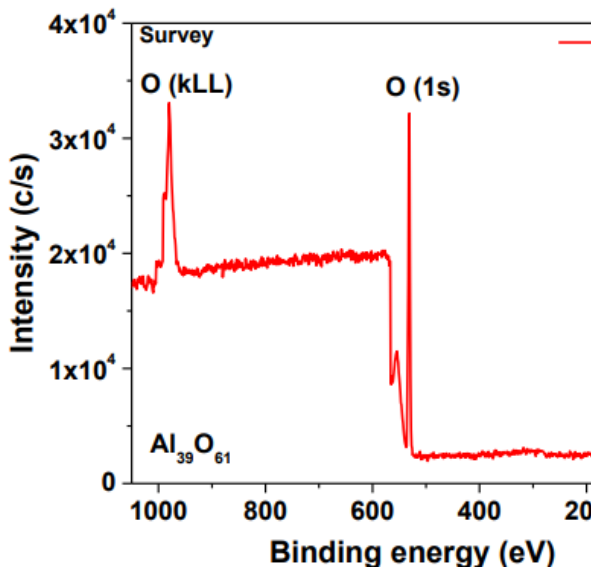
Survey spectrum of Al–O coatings on Si with an R.f. negative bias voltage of around 20 V was obtained. Figures 5a and 5b show the high-resolution spectra for Al(2p) and O(1s), which were modified using Gaussian functions in the same way as for the Si3N4 coating. For Al(2p) and O(1s), there was just one peak at 75.9 and 532.9 eV, respectively, which is consistent with the existence of Al2O3 in both materials [10, 13]. Other than that, contamination of the sample or test chamber may be attributed to the presence of the Al(2s) peak at 121.09 and C(1s) at 254.5 eV. A close approximation was made to the optimal 1.33 and 1.55 ratios by using these values.
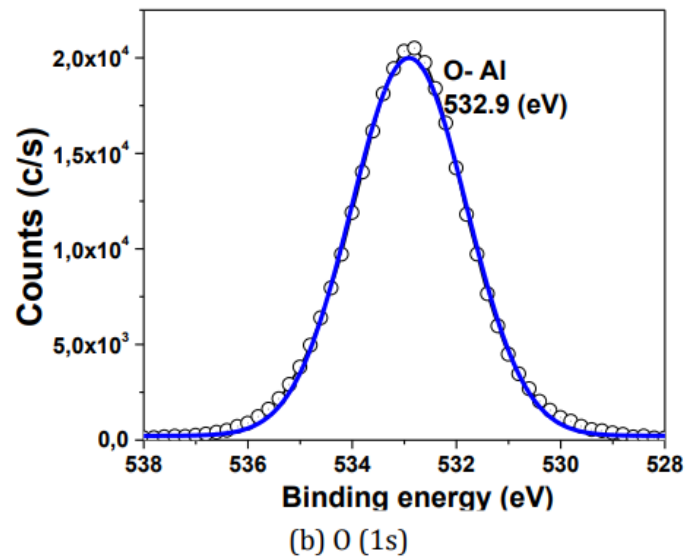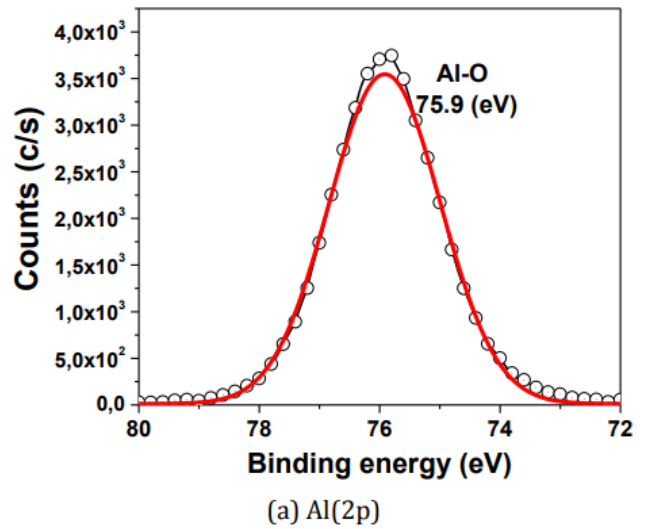
(a) Al(2p)

(b) O (1s)

High-resolution spectrum of (a) A1(2p), and (b) O(1s) from the Al–O coating.

Scanning Electron Microscopy (SEM)

This figure displays the cross section SEM of the [Si3N4/Al2O3]10 multilayer coating consisting of n=10 (200 nm) layers, whereas the figure 6a shows the cross section for the single layer of Si3N4 and Al2O3. Different materials have differing electrical densities, which accounts for their varying contrast. As a result, one material's contrast seems lighter while another material's contrast appears darker; this means the Al2O3 layer has a lighter contrast. As a result, it was found that the coatings were deposited in the correct configuration. There are no obvious fissures or deformations in the coating's transverse section, and no precipitated components or other phases are present in the single layers or multilayer coatings.
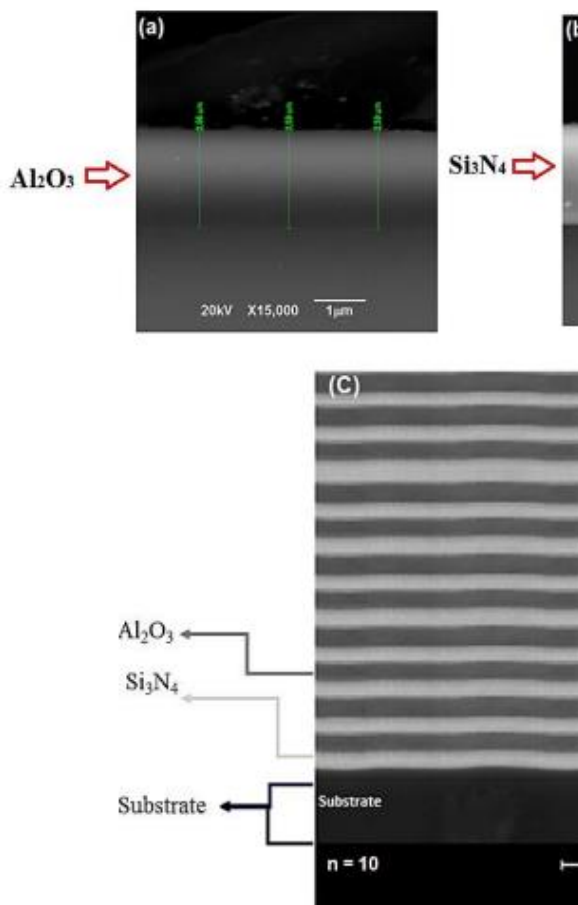
Single layer Si3N4 (a), Al2O3 (b), and n-layer [Si3N4/Al2O3]n (deposited with n = 10) cross-sectional SEM micrographs are shown in the images below.

Atomic Force Microscopy (AFM)

The atomic force microscopy was used to examine the multilayer coatings' surface in relation to the number of bilayers. On Si (100) substrates, AFM pictures of the [Si3N4/Al2O3]n multilayers were captured. A statistical distribution of grain size was performed in an area of 5x5 nm, with the Z range of 0.01 nm, and no-contact mode for (a) n = 1, and (b) (10) (200 nm), (c) n = 30, and (d) n = 70. A statistical analysis scanning probe image processor (SPIP®) was used to acquire roughness and grain size quantitative data from Fig. 7. In Fig. 8a and 8b, these values were displayed as a function of the number of bilayers. A constant overall thickness of 2 nm was used to guarantee that these properties were linked to their intrinsic nature. When comparing the n = 1 (= 1000 nm) and n = 70 (= 29 nm) deposited multilayers, it is obvious that the surface roughness and granule size of the multilayers reduced with increasing bilayer number and decreasing bilayer period, to be exact, a reduction of 49.4% and a reduction of 30.0 percent. They also show how the multilayer with n = 1 was more disordered than the

multilayer   with   70.
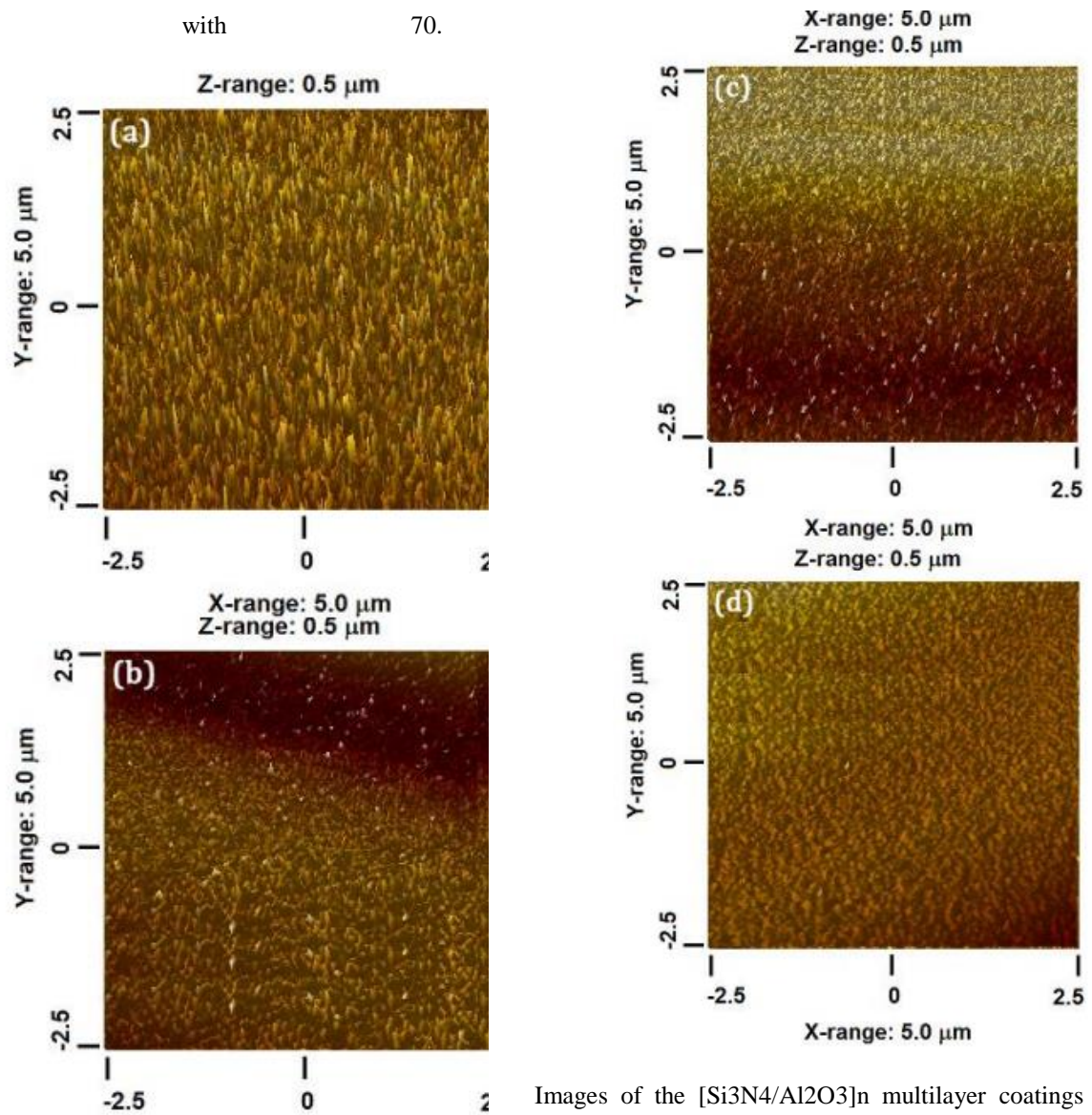
Images of the [Si3N4/Al2O3]n multilayer coatings deposited as a function of the bilayer number and bilayer period (a) n=1, =1000 nm; (b) n=10, =200 nm; (c) n=30, =67 nm; and (d) n=70, =29 nm; Various variables, including the stoppage of grain development when a fresh layer was applied, and the lowering of individual coating thicknesses, promoted a higher number of nucleation sites, contributed to the reduction in grain size. All of these factors resulted in a more compact and dense microstructure, which in turn reduced surface roughness [18]. Because harsh conditions may increase the corrosion susceptibility of thin films, having an uniform surface

might assist lessen that vulnerability [19].

(Er).

(a)
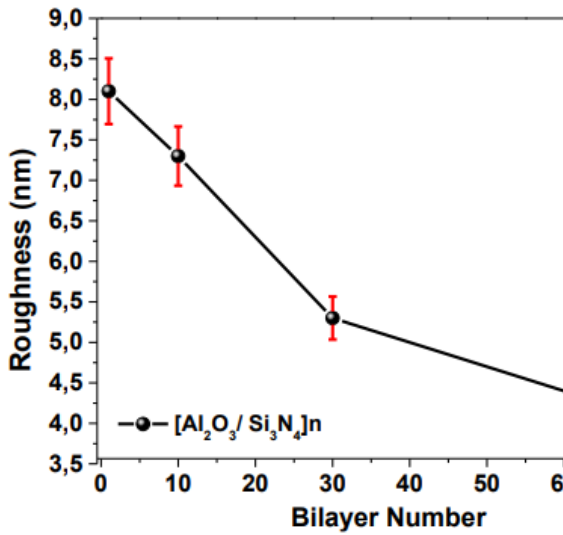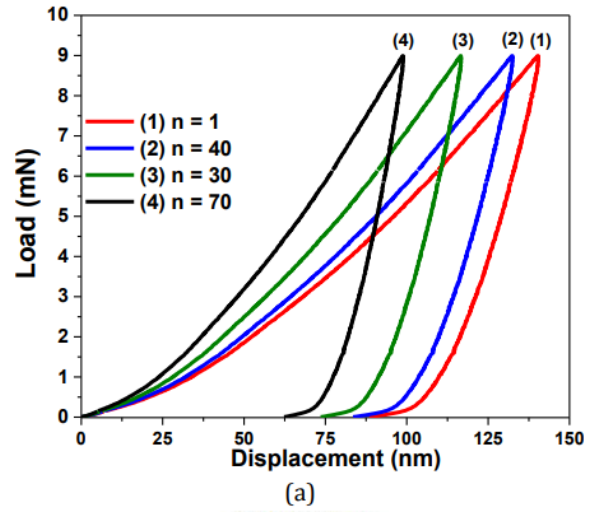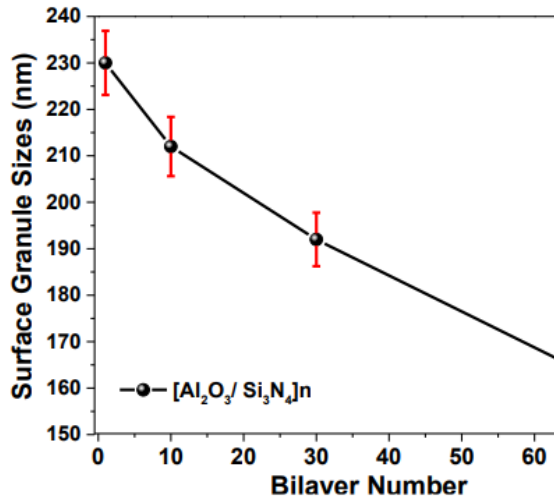
(b)
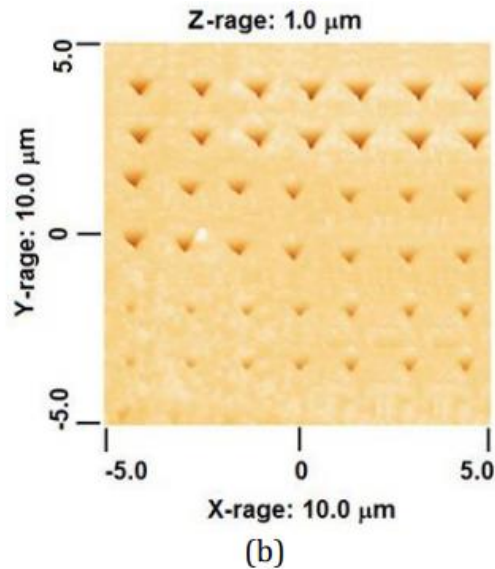
Correlation between the number of bilayers on the surface and the grain size of the surface is examined in this section.
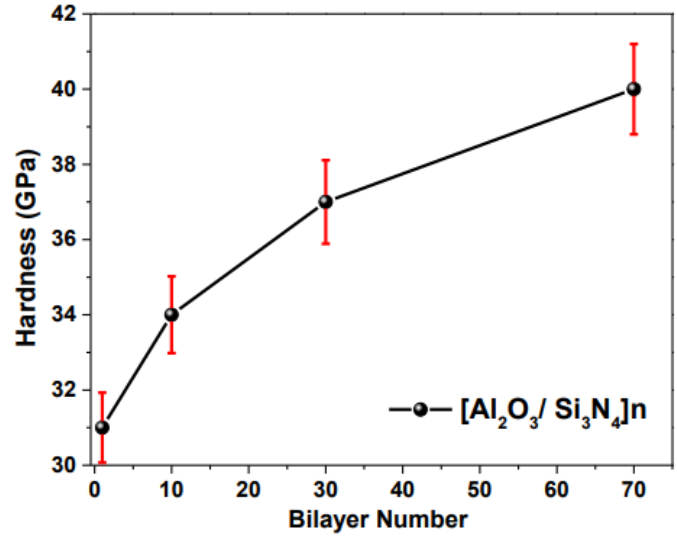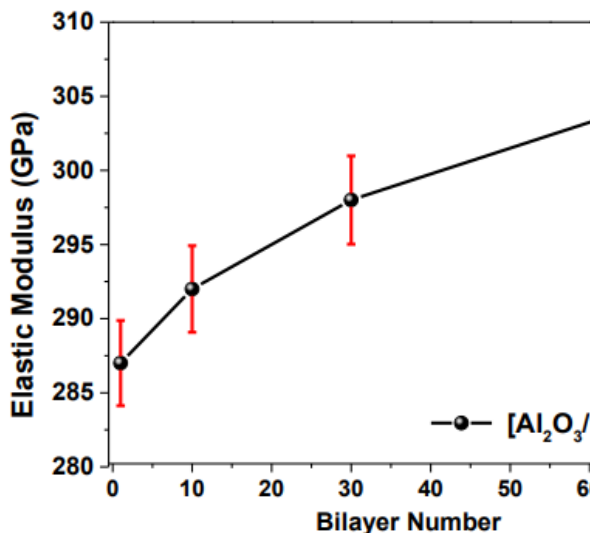
Nanoindentation

the load-displacement curves from the nanoindentation test using a typical Berkovich type indenter are shown in this figure. The AFM picture of the indentation matrix for the multilayer deposited with n=30 (=67 nm) may be seen in Figure 9b. For multilayer coatings placed on AISI 316 steel substrates, the Oliver-Pharr technique [16, 21] was used to determine the hardness and elastic modulus

An AFM picture of the indentation matrix of a [Si3N4/Al2O3]n multilayer deposited with n = 30 and = 67 nm was used to detect nanoindentations in [Si3N4/Al2O3]. This work used nanoindentation experiments to estimate the elastic modulus and hardness, as shown in Fig. 10. The indentations were done at 10% of the overall thickness of the coating so that the substrate would not influence the findings. The following equation (2) [20] was used to adapt the Hall-Petch effect in order to represent the mechanical behaviour of multilayer materials with layer thicknesses ranging from 1 to 100 nm:

$$H_m = H_{(f1+f2)} + k_{IM} \cdot D_t^{-1/2}$$

GPa*m2 units represent the relative contribution of hardness produced by the thickness of the interface between layers 1 and 2, KIM is a constant measuring the hardness of the multilayer as a whole, and Dt is the bilayer period (). Using this model, it is possible to anticipate how hardness behaves across the bilayer period in many multilayer systems. Figs. 10a and 10b show that the elastic modulus and hardness also rose with the bilayer number, reaching values of 287 GPa and 31 GPa, respectively, at 305 and 40 GPa. Figures. Comparing the multilayer with n = 70 (= 29 nm) to n=1 (= 1000 nm), there was a 6.3% increase in elastic modulus and a 29.0% increase in hardness. The rise in the number of interfaces between the Si3N4 and Al2O3 layers may be responsible for this impact, since each new contact acts as a grain limit, according to the Hall-Petch effect [21]. There is a greater critical creep stress associated with the changes in shear modulus of the different materials that make up a multilayer coating, thus dislocations cluster in or slide over these interfaces. In addition, as shown in the AFM studies, this rise in hardness and elastic modulus is also due to a decrease in grain size as the number of bilayers grows (Fig. 8). When a coating has a large number of small grains that have a high boundary grain density per volume (BGD/V), the dislocations generated by stress are blocked, resulting in an increase in the hardness and elastic modulus of the coating [15–16], as well as an increase in the hardness and elastic modulus [17–19]. The coating with 70 bilayers and a nanometric bilayer period (= 29 nm) will have higher mechanical characteristics because of the preceding, as would a coating with more interfaces and smaller grain size [29, 30].


(b)

elastic modulus and hardness of [Si3N4/Al2O3]n multilayers as a function of bilayer number. The plastic deformation resistance (H3/E2) and elastic recovery of multilayers as a function of bilayer number were also obtained from the nanoindentation test (load-depth curve), as shown in Figs. 11a and 11b. Equation (3) was used to compute the elastic recovery:

$$R = \frac{\delta max - \delta p}{\delta max}$$

hmax is the maximal displacement (max) and p is the residual or plastic displacement (hf). The greater the number of bilayers (n), the greater the mechanical qualities of the multilayer coating, as seen by the rise in plastic deformation resistance and elastic recovery. The correlation between this and the XRD findings of structural coherence is obvious (Fig. 1). As a result of the previously indicated surface features, such as the rise in interface number that lowers grain size (Fig. 8), grain boundary density increases and microcrack movement is impeded, the preferred texturization effect was seen. Thus, the coating with n = 70 is more resistant to deformation and has better mechanical properties[16]. The XRD findings showed that the mechanical characteristics of the multilayers with a greater bilayer number improved as a consequence of

186
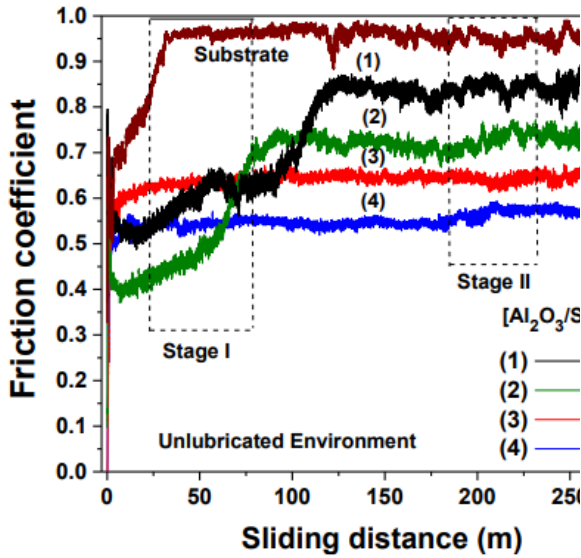
reduced   residual   stress   levels   (Fig.   1)
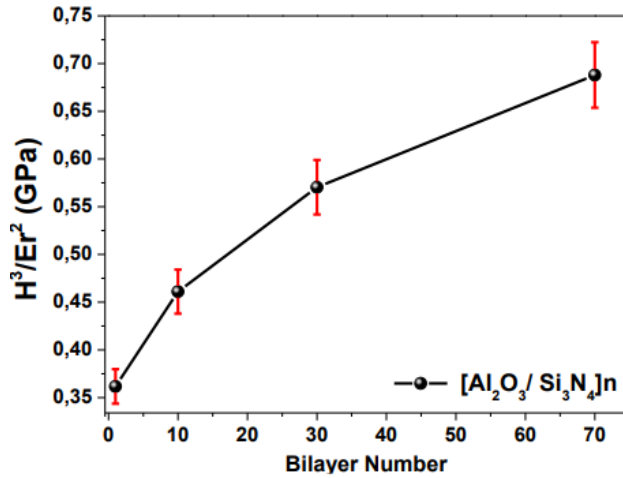
(a)
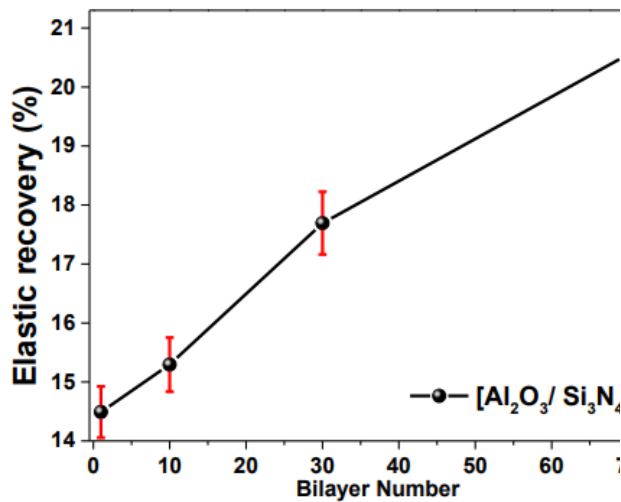
Surface   properties   for   the   [Si3N4/Al2O3]n multilayers   coatings: (a)   Plastic   deformation resistance and (b) Elastic recovery as a function of the bilayer number.
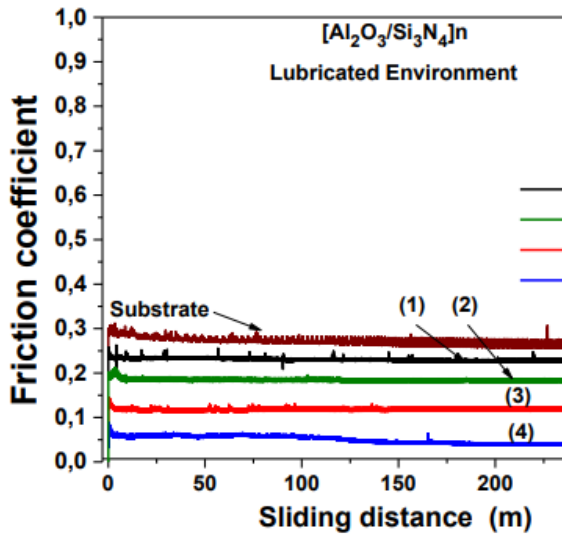
Pin on disk analysis

The pin-on disc approach was used in a non-lubricated and lubricated environment to investigate the tribological behaviour of the [Si3N4/Al2O3]n multilayer systems. All of the multilayers with varying bilayer numbers and the uncoated substrate are shown in Fig. 12 as friction coefficients, and it is clear that in the absence of lubricant, all of the curves displayed a two-stage behaviour (Fig. 12a). For the n = 30 and n = 70 coatings, the length of those phases is clearly different, presumably because to the greater

shift in periodicity when increasing the bilayer number. Beginning with the first contact, friction coefficients are lower in stage I (known as the "starting phase") because the asperities on both sides of a tribological pair come into touch with each other, resulting in interferential friction. The friction coefficient quickly rises as a result of the accumulation of wear particles, known as debris, on the surface. As the asperities of the two surfaces are smoothed, the coefficient of friction is reduced and stabilised. It's at this running-in stage II that the asperities are annihilated and coating flaws arise as a result of the frictional conflict between the interferential and adhesive processes. Lower sliding distances in Stage II begin when the bilayer number grows in this stage. Higher bilayer number surfaces have better mechanical qualities and reduced roughness, resulting in less wear particles in the surface when tested tribologically. As a result, the friction coefficient stabilises much more quickly in comparison to coatings with a lower bilayer count. In addition, a distinct difference between the non-lubricated and lubricated friction coefficients of multilayer coatings may be seen when comparing the two (Fig. 12b). Furthermore, because of the decreased friction coefficient and the fact that it is kept constant across a wide area, the curves are accelerated practically instantly to stage II. lubrication minimises the incidence of asperity contact, reduces surface shear pressures, and decrease wear rate [32]. Due to its huge number of interfaces and their effects, the multilayer with n = 70 had the greatest performance. As a consequence, the optimum tribological result for stainless steel device protection is achieved by combining steels coated with nanometric [Si3N4/Al2O3]n multilayers made

of Si3N4 and Al2O3 layers.

characteristics of the coating in the following equation (4):

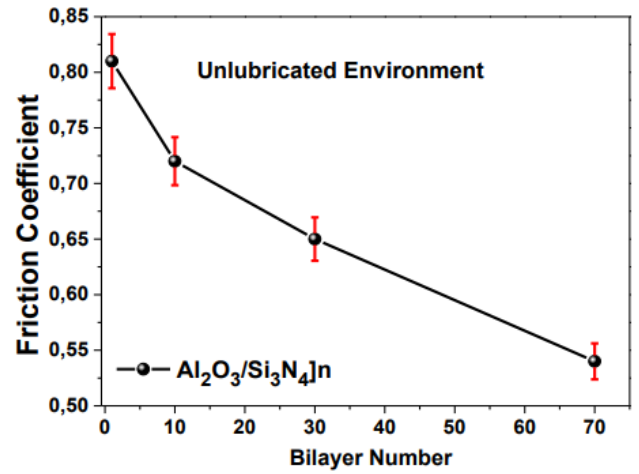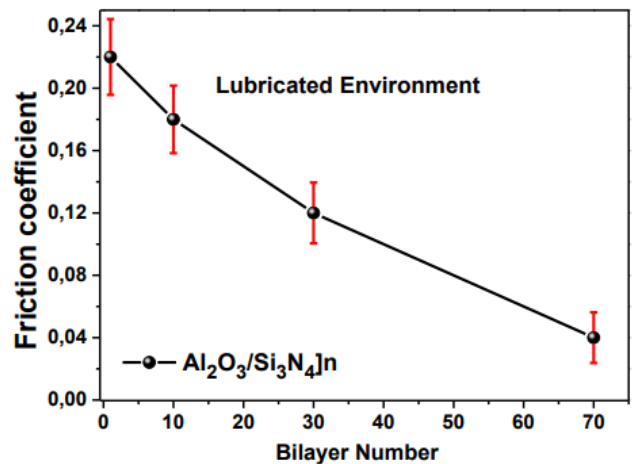$$\mu = \frac{F_f}{F_n} = C_k \cdot \frac{R_{(s,a)}}{\sigma t_{(H,Er)}}$$

(a)

(a)

(b)

All [Si3N4/Al2O3]n multilayer coatings (a) Friction coefficient under non-lubricated conditions and (b) Friction coefficient under lubricated conditions Using a non-lubricated environment, Figure 13 shows how the friction coefficient decreases over time as the number of bilayers increases. This shows that the lowest friction coefficient was found in the multilayer deposited with bilayer number n = 70 (= 29 nm), which was 33.3 percent less frictional than the multilayer with bilayer number n = 1 (= 1000 nm). Archard [33] established a mechanical friction model, which connects the contribution of the surfaces in contact (roughness) and the elastic-plastic

Non-lubricated and lubricated environments: [Si3N4/Al2O3]n multilayer coatings' friction coefficients as a function of bilayer number. A constant called Ck depends on test circumstances, and R(s,a) is the coating's roughness (which might be quadratic for micron-scale or arithmetic for macroscale roughness), where t is an elastic-plastic property variable that takes into consideration R(s,aroughness.)'s (hardness, H or elastic modulus, Er). The friction coefficient tends to decrease and remain stable over long sliding distances when the

coating's surface has a low roughness (Fig. 8b) and a high hardness (Fig. 10b) according to Archard's model [29, 34], which is in perfect agreement with the previous results when the coating's counterpart is less hard (100Cr6 pin ball). Fig. 13b shows the friction coefficient in a lubricated environment, where the friction values were lowered to exceptionally low levels due to the ideal combination of the multilayers and the lubrication effect (Fig. 13). Although hardness has been considered one of the most important material qualities that correlate with wear resistance, substantial evidence suggests that the elastic modulus might also have a significant impact on wear behaviour. It has been established by various authors that the H3/E2 relationship is the most appropriate parameter to predict resistance to wear, in particular, the plastic deformation resistance, which is linked to hardness (H) and elastic modulus (E) in the form of H3/E2 (Fig. 11a). The wear resistance of the coatings was also assessed using the Pin-On-Disk testing. As shown in Figure 14, scanning electron microscopy (SEM) was used to examine the wear track to determine what kind of wear was occurring on the surface. [Si3N4/Al2O3]n multilayers showed satisfactory results, with reasonably smooth and continuous wear patterns, thanks to their nanometric size. In the wear tracks, several tribological events could be seen, such as the formation of adhesion between the coated surface and the steel pin (counterpart), which resulted in the delamination of a layer. As a result of the delamination of coating particles and the subsequent hardening of their counterparts by plastic deformation (debris), abrasion was seen on the coated surface [31].



(b) n = 10, Λ = 200

(c) n = 30, Λ = 67 nm

(d) n = 70, Λ = 29 nm

(a) Steel Uncoated
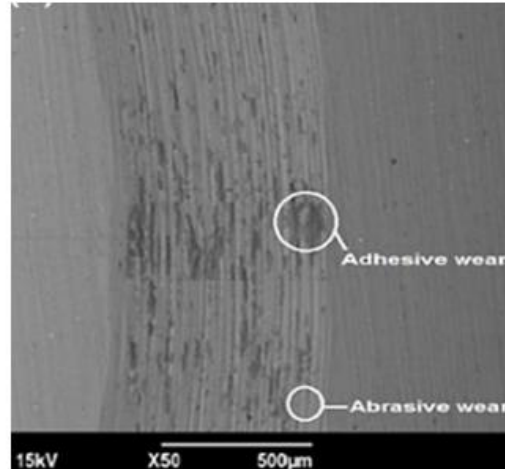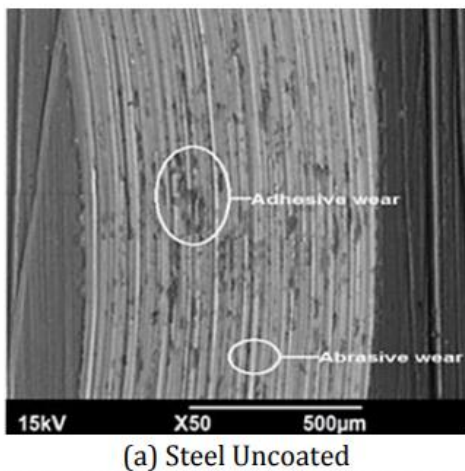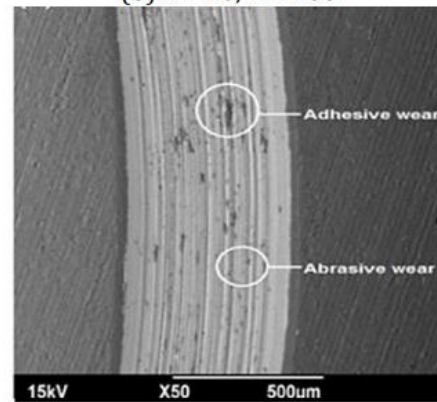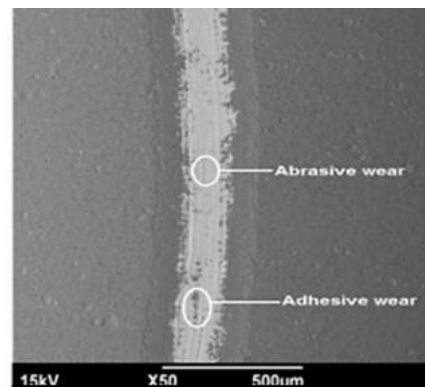
A series of bilayer number and bilayer period () vs wear track SEM micrographs for the [Si3N4/Al2O3]n multilayer coatings are shown in the following images: a, b, c, and d, respectively. Even the multilayer with only one layer (n = 1) had a wear track that was deeper and broader than that of the other multilayers. This suggests that the material was suddenly ruptured, as opposed to the other

189

multilayers, which had a more gradual breakdown. Adhesion and abrasion processes are often implicated in the development of these kinds of marks. Multilayers with a large bilayer count (n) or low periodicity revealed a totally different response; wear and track size decreased as the number of bilayers grew, proving that layer count had an impact on wear resistance.. It was found that in dynamic mode, against 100Cr6 steel balls (the counterpart), the multi-layer with a n = 70 (= 29 nm) was superior at resisting wear owing to the combination of high hardness and a low friction coefficient that the multi-layer structure with a large number of interfaces provided. The wear trails are shown in 3D in Figure 15. When the number of bilayers is increased, wear may be seen in a non-lubricated environment. As mechanical characteristics improved, the friction coefficient declined and the coating resistance rose, indicating that the track's depth and breadth reduced. The tribological test results for the [Si3N4/Al2O3]n multilayer coating show the effect of bilayer number on the breadth and depth of the track. Figs. 10-11 show a decrease in geometrical wear when the elastic modulus and plastic deformation resistance increase, both of which lessen the likelihood of microcrack generation and the delamination processes that occur as a consequence. Figures 16a and 16b show that the coating with the lowest number of bilayers had the greatest wear effect, with an average track width of 3.03 mm and depth of 2.36 nm, while the coating with the highest number of bilayers n = 70, (= 29 nm) had the least wear with a track width of 1.12 mm and depth of 0.215nm, respectively. This shows a reduction of 63% and 91.2 %.
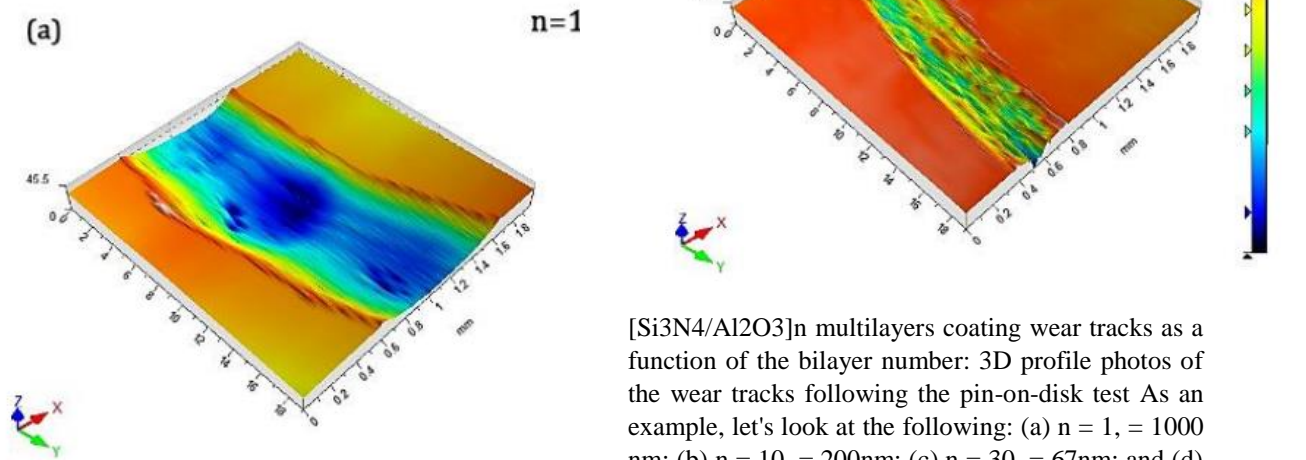
[Si3N4/Al2O3]n multilayers coating wear tracks as a function of the bilayer number: 3D profile photos of the wear tracks following the pin-on-disk test As an example, let's look at the following: (a) n = 1, = 1000 nm; (b) n = 10, = 200nm; (c) n = 30, = 67nm; and (d)

n = 70, = 29nm;

(a)


(b)
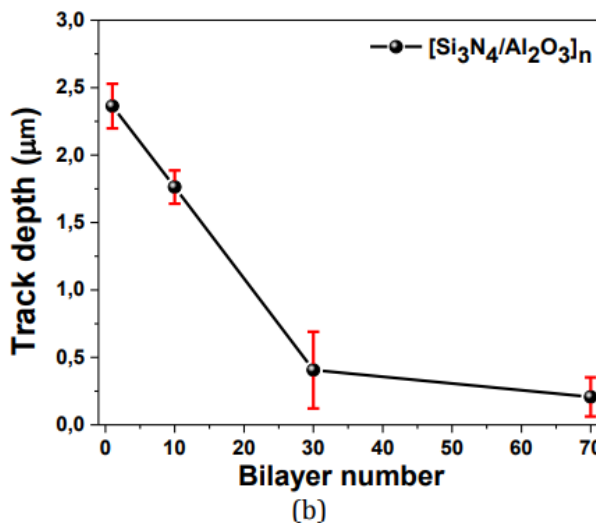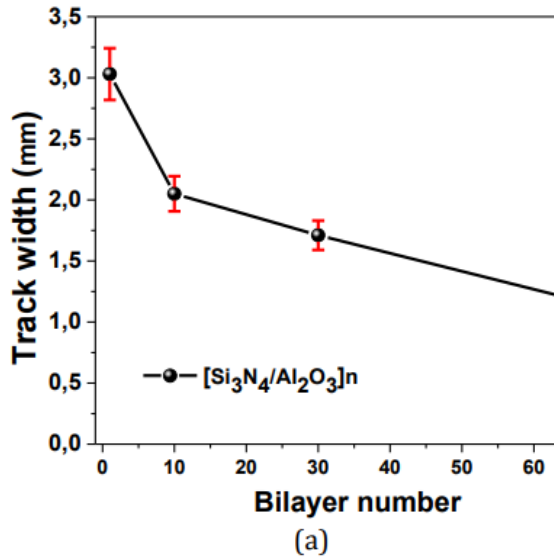
For [Si3N4/Al2O3]n multilayers coatings, geometric measurements of wear tracks following the pin-on-disk test as a function of the bilayer number: Both the width and depth of the track

Scratch test analysis

Scratch testing was used to evaluate the adherence of the nano composite [Si3N4/Al2O3]n multilayer coatings. Fig. 17 shows the scratch test results for each multilayer. If you take into consideration two terms: LC1 is the low critical load where initial fractures begin to form due to cohesive failure; and LC2 is the higher critical load where the first delamination occurs in the border of a scratch mark due to adhesive failure. As the load stabilises in relation to the friction coefficient, several critical loads were identified. In the first stabilisation, the adhesive failure is attributed with stabilising the structure. [33-37]

(b)

(c)

(d)
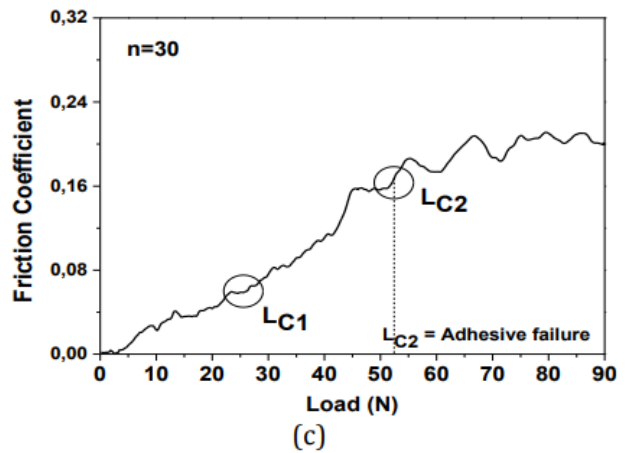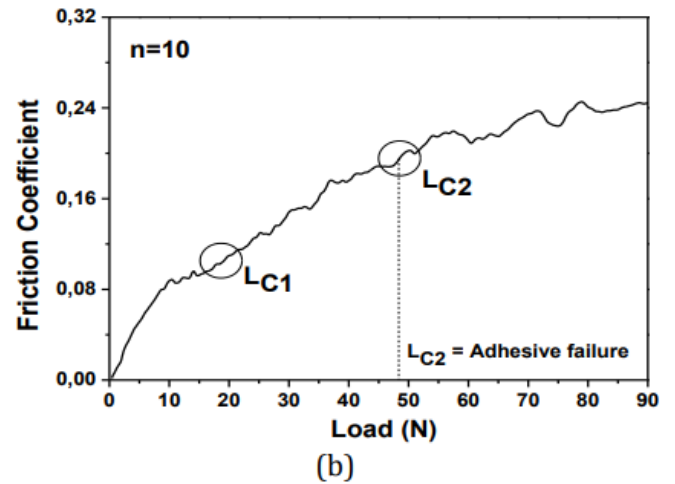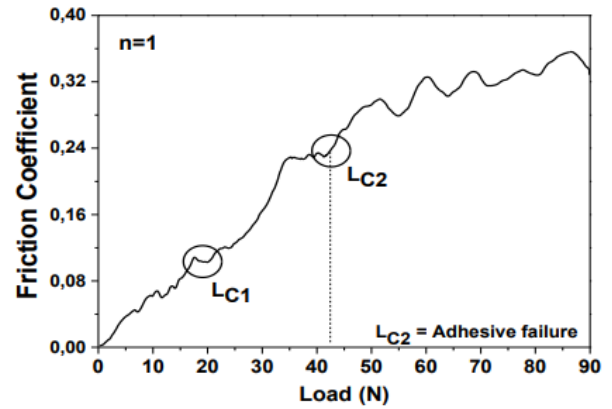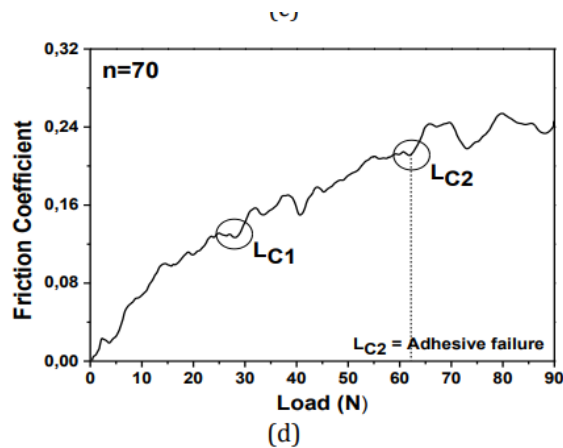
[Si3n4/Al2o3]n multilayer coating scratch test results: (a) n = 1, (b) n = 10, (c) n = 30, and (d) n = 70. The friction coefficient as a function of the applied load was determined from the scratch test data for all [Si3n4/Al2o3]n multilayer coatings.

Data from figure 17 was used to create Fig. 18, which illustrates how the superior critical load (LC2) varies as the bilayer number increases. There was a correlation between increasing the number of bilayers and increasing the critical load, which means that the multilayer with n = 70 (= 29 nm) had the best multilayer adhesion in comparison to the other [Si3N4/Al2O3]n multilayers, with a critical load of 62 N, resulting in a 47.6 percent increase in comparison with n = 1 (= 1000 nm). The lower residual stress levels in the multilayers with a greater number of bilayers, as seen in the XRD data, may have contributed to this behaviour (Fig. 1).
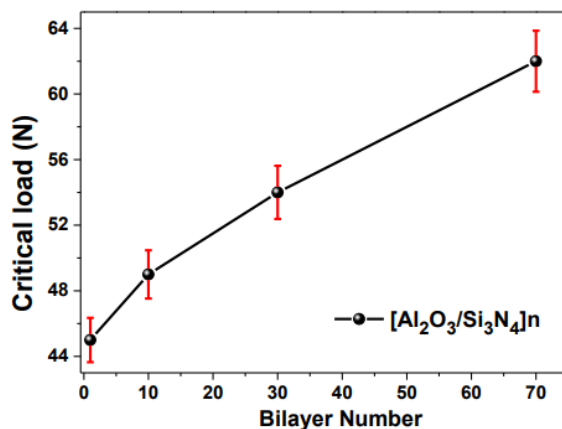
Critical load as a function of the bilayer number for the [Si3N4/Al2O3]n multilayer coatings.

CONCLUSIONS

The structural study indicated that the multilayer coatings [Si3N4/Al2O3]n displayed a hexagonal crystalline structure with favoured orientations (101) and (209) for the Si3N4 and Al2O3 layers respectively. AFM studies demonstrated a decrease of grain size and roughness of about 30.0 percent and 49.4 percent , respectively, while increasing the bilayer number from n = 1 to n = 70. The multilayer with the greatest bilayer number (n = 70) and lowest bilayer period (Λ = 200) acquired a hardness of 40 GPa and an elastic modulus of 305 GPa, demonstrating a 29.0 percent and 6.3 percent improvement, respectively, when compared to the multilayer with the lowest bilayer number (n = 1). Tribological results show an approximate 33.3 percent decrease in friction coefficient (0.54) within a non-lubricated environment and 81.8 percent decrease in friction coefficient under lubricated environment for the multilayer with the highest bilayer number (n = 70) when compared to the lowest (n = 1), Scratch results showed a 47.61 percent increase in critical load was needed for adhesive failure, indicating that these multilayer coatings may be a promising material to be applied in the food and pharmaceutical industries

REFERENCES

[1] C.H. Ortiz, H.D. Colorado, W. Aperador, A. Jurado, Influence of the number of bilayers on the mechanical and tribological properties in [TiN/TiCrN]n multilayer coatings deposited by magnetron sputtering, Tribology in Industry, vol. 41, no. 3, pp. 330–343, 2019, doi: 10.24874/ti.2019.41.03.03

[2] D.D. Kumar, N. Kumar, S. Kalaiselvam, S. Dash, R. Jayavel, Wear resistant super-hard multilayer transition metal-nitride coatings, Surfaces and

Interfaces, vol. 7, pp. 74–82, 2017, doi: 10.1016/j.surfin.2017.03.001

[3] J.C. Caicedo, A. Guerrero, W. Aperador, Determination of multilayer effect evidence on metal carbon-nitride system, Journal of Alloys and Compounds, vol. 785, pp. 178–190, 2019, doi: 10.1016/j.jallcom.2019.01.151

[4] K. Kishi, M.W. Roberts, Adsorption of nitrogen and ammonia by polycrystalline iron surfaces in the temperature range 80–290 K studied by electron spectroscopy, Surface Science, vol. 62, iss. 1, pp. 252–266, 1977, doi: 10.1016/0039- 6028(77)90441-1

[5] V. Bonu, M. Jeevitha, V. Praveen Kumar, G. Srinivas, Siju, H.C. Barshilia, Solid particle erosion and corrosion resistance performance of nanolayered multilayered Ti/TiN and TiAl/TiAlN coatings deposited on Ti6Al4V substrates, Surface and Coatings Technology, vol. 387, pp. 125531, 2020, doi: 10.1016/j.surfcoat.2020.125531

[6] S.H. Shin, J.W. Cho, S.H. Kim, Structural investigations of CaO-CaF2-SiO2-Si3N4 based glasses by Raman spectroscopy and XPS considering its application to continuous casting of steels, Materials and Design, vol. 76, pp. 1–8, 2015, doi: 10.1016/j.matdes.2015.03.035

[7] S. Yadav, S. Sahoo, Interface study of thermally driven chemical kinetics involved in Ti/Si3N4 based metal-substrate assembly by X-ray photoelectron spectroscopy, Applied Surface Science, 2020, doi: 10.1016/j.apsusc.2020.148465

[8] M. Pettersson, M. Bryant, S. Schmidt, H. Engqvist, R.M. Hall, A. Neville, C. Persson, Dissolution behaviour of silicon nitride coatings for joint replacements, Materials Science and Engineering: C, vol. 62, pp. 497–505, 2016, doi: 10.1016/j.msec.2016.01.049

[9] P.H.C. Camargo, K.G. Satyanarayana, F. Wypych, Nanocomposites: Synthesis, structure, properties and new application opportunities, Materials Research, vol. 12, no. 1, pp. 1–39, 2009, doi: 10.1590/S1516-14392009000100002

[10] A. Pogrebnjak, K. Smyrnova, O. Bondar, Nanocomposite Multilayer Binary Nitride Coatings Based on Transition and Refractory Metals, Structure and Properties, Coatings, vol. 9, iss. 3, pp. 155, 2019, doi: 10.3390/coatings9030155

[11] S. Zimowski, T. Moskalewicz, B.G. Wendler, Analysis of the tribological properties of TiN/Si3N4 nanocomposite coating in sliding contact with ceramic, steel, and polymer counterpart, Tribologia, vol. 4, pp. 125, 2017.

[12] I. Mohammadi, A. Afshar, S. Ahmadi, Al2O3/Si3N4 nanocomposite coating on aluminum alloy by the anodizing route: Fabrication, characterization, mechanical properties and electrochemical behavior, Ceramics International, vol. 42, iss. 10, pp. 12105–12114, 2016, doi: 10.1016/j.ceramint.2016.04.142

[13] M. Michalak, L. Łatka, P. Sokołowski, A. Niemiec, A. Ambroziak, The microstructure and selected mechanical properties of Al2O3 + 13 wt % TiO2 plasma sprayed coatings, Coatings, vol. 10, iss. 2, 39–45, 2020, doi: 10.3390/coatings10020173

[14] C. Escobar, M. Villarreal, J.C. Caicedo, W. Aperador, H.H. Caicedo, P. Prieto, Diagnostic of corrosionerosion evolution for [Hf-Nitrides/V-Nitrides]n structures, Thin Solid Films, vol. 545, pp. 194–199, 2013, doi: 10.1016/j.tsf.2013.07.081

[15] G. Pradhaban, P. Kuppusami, D. Ramachandran, K. Viswanathan, R. Ramaseshan, Nanomechanical properties of TiN/ZrN multilayers prepared by pulsed laser deposition, Materials Today: Proceedings, vol. 3, iss. 6, pp. 1627–1632, 2016, doi: 10.1016/j.matpr.2016.04.052

[16] J.C. Caicedo, G. Cabrera, H.H. Caicedo, C.Amaya, W. Aperador, Nature in corrosion-erosion surface for [TiN/TiAlN]n nanometric multilayers growth on AISI 1045 steel, Thin Solid Films, vol. 520, iss. 13, pp. 4350–4361, 2012, doi: 10.1016/j.tsf.2012.02.061

[17] S. Prasanna, G. Krishnendu, S. Shalini, P. Biji, G. Mohan Rao, S. Jayakumar, R. Balasundaraprabhu, Materials Science in Semiconductor Processing Composition, structure and electrical properties of DC reactive magnetron sputtered Al2O3 thin films, Materials Science in Semiconductor Processing, vol. 16, iss. 3, pp. 705–711, 2013, doi: 10.1016/j.mssp.2012.12.012

[18] S. Prasanna, G. Krishnendu, S. Shalini, P. Biji, G.M. Rao, S. Jayakumar, R. Balasundaraprabhu, Composition, structure and electrical properties of DC reactive magnetron sputtered Al2O3 thin films, Materials Science in Semiconductor Processing, vol.

16, iss. 3, pp. 705–711, 2013, doi: 10.1016/j.mssp.2012.12.012

[19] A.A. Pradhan, S.I. Shah, K.M. Unruh, Reactive sputter deposition of alumina thin films using a hollow cathode sputtering source, Review of Scientific Instruments, vol. 73, iss. 11, pp. 3841–3845, 2002, doi: 10.1063/1.1512340

[20] J.C. Caicedo, G . Bejarano, M.E. Gómez, P. Prieto, C. Cortéz, J. Muñoz, Nanostructured multilayers of TiN/ZrN obtained by magnetron sputtering, Physica Status Solidi C, vol. 4, iss. 11, pp. 4127– 4133, 2007, doi: 10.1002/pssc.200675912

[21] Y.W. Bao, W. Wang, Y.C. Zhou, Investigation of the relationship between elastic modulus and hardness based on depth-sensing indentation measurements, Acta Materiala, vol. 52, iss. 18, pp. 5397–5404, 2004, doi: 10.1016/j.actamat.2004.08.002

[22] ASTM G99-17, Standard Test Method for Wear Testing with a Pin-on-Disk Apparatus, 2017.

[23] ASTM G171–03, Standard Test Method for Scratch Hardness of Materials Using a Diamond Stylus, 2003.

[24] I. Iatsunskyi, M. Kempiński, M. Jancelewicz, K. Załęski, S. Jurga, V. Smyntyna, Structural and XPS characterization of ALD Al2O3 coated porous silicon, Vacuum, vol. 113, pp. 52–58, 2015, doi: 10.1016/j.vacuum.2014.12.015

[25] C. Zhuang, J. Zhao, F. Jia, C. Guan, Z. Wu, Y. Bai, X. Jiang, Tuning bond contents in B–C–N films via temperature and bias voltage within RF magnetron sputtering, Surface and Coatings Technology, vol. 204, iss. 5, pp. 713–717, 2009, doi: 10.1016/j.surfcoat.2009.09.031

[26] C. Zhuang, J. Zhao, F. Jia, C. Guan, Z. Wu, Y. Bai, X. Jiang, Tuning bond contents in B–C–N films via temperature and bias voltage within RF

pr.2019.04.218

magnetron sputtering, Surface and Coatings Technology, vol. 204, iss. 5, pp. 713–717, 2009, doi: 10.1016/j.surfcoat.2009.09.031

[27] A.A. Vereschaka, S.N. Grigoriev, Study of cracking mechanisms in multi-layered composite nanostructured coatings, Wear, vol. 378–379, pp. 43–57, 2017, doi: 10.1016/j.wear.2017.01.101

[28] S. Nikkhah, H. Mirzadeh, M. Zamani, Improved mechanical properties of mild steel via combination of deformation, intercritical annealing, and quench aging, Materials Science and Engineering A, vol. 756, pp. 268–271, 2019, doi: 10.1016/j.msea.2019.04.071

[29] Z.B. Qi, P. Sun, F.P. Zhu, Z.C. Wang, D.L. Peng, C.H. Wu, The inverse Hall-Petch effect in nanocrystalline ZrN coatings, Surface and Coatings Technology, vol. 205, iss. 12, pp. 3692–3697, 2011, doi: 10.1016/j.surfcoat.2011.01.021

[30] L. Ipaz, J.C. Caicedo, J. Esteve, F.J. EspinozaBeltran, G. Zambrano, Improvement of mechanical and tribological properties in steel surfaces by using titanium-aluminum/titaniumaluminum nitride multilayered system, Applied Surface Science, vol. 258, iss. 8, pp. 3805–3814, 2012, doi: 10.1016/j.apsusc.2011.12.033

[31] S.-K. Tien, J.-G. Duh, Effect of heat treatment on mechanical properties and microstructure of CrN/AlN multilayer coatings, Thin Solid Films, vol. 494, iss. 1-2, pp. 173–178, 2006, doi: 10.1016/j.tsf.2005.08.198

[32] I. Hutchings, P. Shipway, Sliding wear, Tribology: Friction and Wear of Engineering Materials, pp. 107–164, 2017, doi:10.1016/B978-0-08- 100910-9.00005-2

[33] J. Sunil, J. Godwin, C.M. Selvam, Roles of nanomaterials at the rubbing interface of mechanical systems, Materials Today: Proceedings, vol. 21, pp. 184–188, 2020, doi: 10.1016/j.mat